Supporting Information

Beyond Fullerenes: Design of Non-fullerene Acceptors for Efficient Organic Photovoltaics

Haiyan Li,[†] Taeshik Earmme,[†] Guoqiang Ren,[†] Akinori Saeki,[‡,§] Saya Yoshikawa,[‡] Nishit M. Murari,[†] Selvam Subramaniyan,[†] Matthew J. Crane,[†] Shu Seki,[‡] and Samson A. Jenekhe[*,†]

[†]Department of Chemical Engineering and Department of Chemistry, University of Washington, Seattle, Washington 98195-1750, USA.

[‡]Department of Applied Chemistry, Graduate School of Engineering, Osaka University, 2-1 Yamadaoka, Suita, Osaka 565-0871, Japan.

[§]PRESTO, Japan Science and Technology Agency (JST), 4-1-8 Honcho Kawaguchi, Saitama 332-0012, Japan.

Table of Contents

1. Methods

1.1. Characterizations

^{1}H NMR and ^{13}C NMR spectra were recorded on a Bruker AV500 at 500 MHz using deuterated chloroform ($CDCl_3$) as the solvent. Mass spectra were obtained from Bruker AutoFlex II Matrix-Assisted LASER Desorption Ionization - Time of Flight Mass Spectrometer (MALDI-TOF) using benzo[α]pyrene as a matrix recorded in a (+)-reflector mode . Thermogravimetric analyses of the molecules were conducted on a TA Instrument model Q50TGA. A heating rate of 10˚C/min under a flow of N_2 was used with runs conducted from room temperature to 600 ˚C. Differential scanning calorimetry (DSC) analysis was performed on a TA Instruments Q100 under N_2 at a heating rate of 20 ˚C/min. The second-heating and corresponding cooling DSC scans were reported. X-Ray Diffraction (XRD) data were collected from a Bruker-AXS D8 Focus diffractometer with Cu-K-α beam (40 kV, 40 mA) in theta-2-theta scans (0.02 Å step size, 1 sec/step). Bright-field transmission electron microscopy (BF-TEM) imaging was conducted on an FEI Tecnai G^2 F20 TEM operating at 200 kV (point resolution: 0.23 nm; line resolution: 0.11 nm). A 0.031 mm^2 aperture was used for selected area electron diffraction (SAED). TEM images were acquired with a CCD camera and recorded with Gatan DigitalMicrograph software. Cyclic voltammetry was performed on an EG&G Princeton Applied Research potentiostat/galvanostat (model 273A). Data were analyzed by using a Model 270 Electrochemical Analysis System Software on a PC computer. A three-electrode cell was used, using platinum wire electrodes as both counter and working electrode. Silver/silver ion (Ag in 0.1 M $AgNO_3$ solution, Bioanalytical System, Inc.) was used as a reference electrode. Ferrocene was used as an internal standard. A layer of sample was deposited onto the working electrode. A solution of tetrabutylammonium hexafluorophosphate (Bu_4NPF_6) in acetonitrile (0.1 M) was used as the electrolyte. The LUMO energy level was calculated from the reduction onset potential using LUMO = – 4.8 eV – E_{red}^{onset}. The HOMO energy level of DBFI-T was calculated from the oxidation onset potential using HOMO = -4.8 eV – E_{ox}^{onset}. All solutions were purged with argon for 20 min before each experiment. UV-vis absorption spectra were collected on a Perkin-Elmer model Lambda 900 UV/vis/near-IR spectrophotometer. Optical band gap (E_g) was estimated from the absorption edge of thin film samples. The HOMO energy level of BFI-P2 was calculated using HOMO = LUMO-E_g since no apparent oxidation wave was detected under the experimental conditions. Calculations for the (gas-phase) molecules were carried out using the Gaussian (Gaussian 09, Revision A.02) suite of programs[1] with density functional theory (DFT) at a B3LYP/6-31G(d) level. Vertical electronic transitions to the low-lying excited states were

evaluated at the neutral ground state geometries and the anion state using time dependent-DFT (TD-DFT) at the same level.

1.2. Fabrication and Characterization of Field-Effect Transistors

Field-effect transistors were fabricated on a heavily n-doped silicon substrate with thermally grown silicon dioxide gate insulator (200 nm). The substrates were cleaned by ultrasonication with acetone and isopropyl alcohol and dried by flow of nitrogen. The surface of a silicon dioxide substrate was further cleaned by plasma and treated with octyltrichlorosilane (OTS8) to form a hydrophobic self-assembled monolayer (SAM). DBFI-T and BFI-P2 were deposited by spin-coating from a solution in chloroform (10 mg/mL) onto the substrates with pre-patterned bottom-contact electrodes. The devices were annealed at various temperatures under argon environment. Top-contact devices (DBFI-T and BFI-P2) were finished by evaporating metal gold electrodes with a channel width of 1000 μm and a length of 100 μm. Electrical characteristics of the devices were measured by using an HP4145B semiconductor parameter analyzer under nitrogen atmosphere. The saturation field-effect mobility (μ_e^{sat}) and threshold voltage (V_t) were calculated by using plots of $I_{ds}^{1/2}$ vs. V_{gs} in a forward scan with V_{ds} = 80 V and a saturation-region equation, $I_{ds}=\mu_e^{sat}WC_i (V_{gs}–V_t)^2 (2L)^{-1}$.

1.3. Space-Charge-Limited Current (SCLC) Measurement

Current-voltage (J-V) characteristics of the SCLC devices were measured by using a HP4155A semiconductor parameter analyzer (Yokogawa Hewlett-Packard, Tokyo). The electron mobility was extracted by fitting the J-V curves in the near quadratic region according to the modified Mott-Gurney equation[2],

$$J = \frac{9}{8}\varepsilon\varepsilon_0\mu\frac{V^2}{L^3}exp\left(0.89\beta\frac{\sqrt{V}}{\sqrt{L}}\right)$$

where J is the current density, ε_0 is the permittivity of free space, ε is the relative permittivity, μ is the zero-field mobility, V is the applied voltage, L is the thickness of active layer, and β is the field-activation factor.

2. Supporting Figures

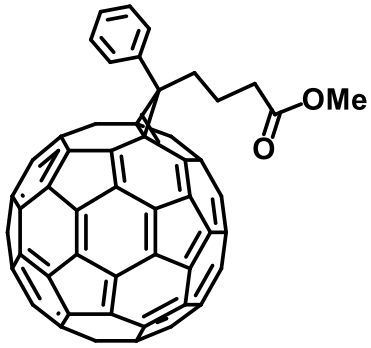

Figure S1. Molecular structure of $PC_{60}BM$.

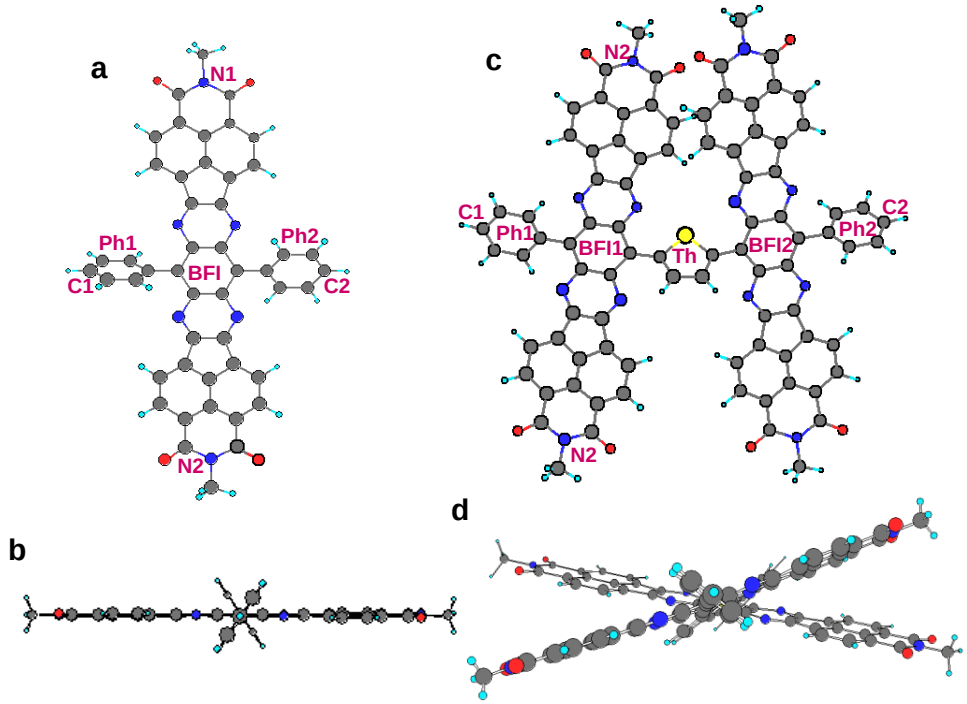

Figure S2. Top and side view of the optimized geometries using DFT calculations at the B3LYP/6-31G(d) level (2-decyltetradecyl groups were replaced with methyl groups): (a and b) BFI-P2, (c and d) DBFI-T.

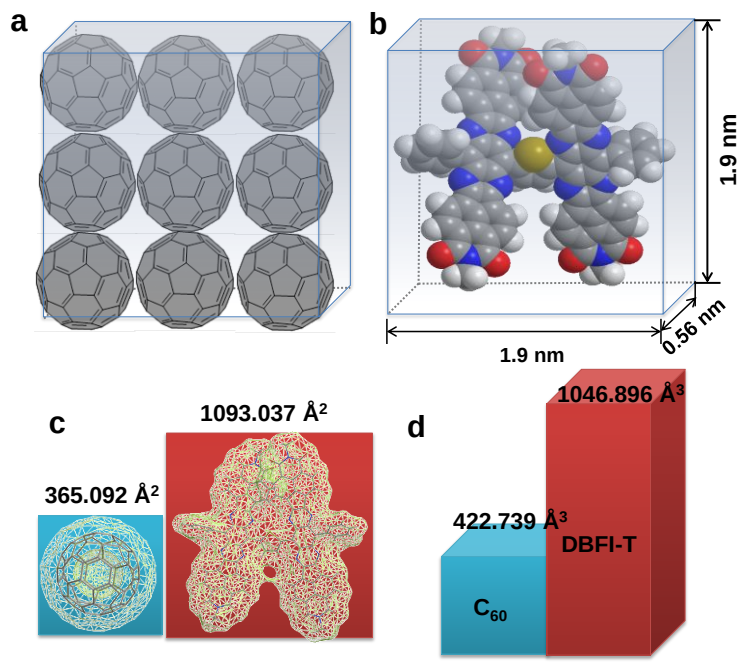

Figure S3. Comparison of the size (a and b), Connolly molecular area (c) and molecular volume (d) of DBFI-T to that of C_{60}.

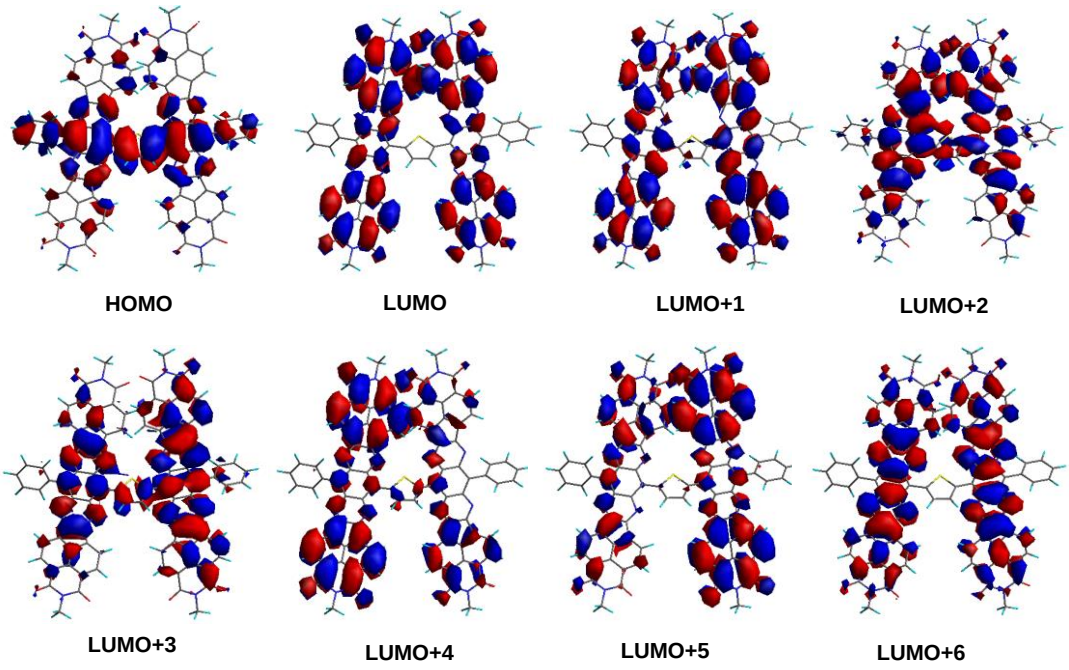

Figure S4. Pictorial representations of the frontier molecular orbitals of DBFI-T from the DFT calculations (B3LYP/6-31G(d), 2-decyltetradecyl groups were replaced with methyl groups).

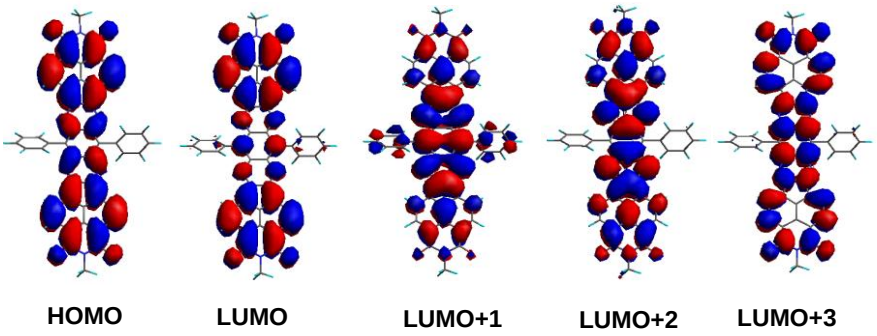

Figure S5. Pictorial representations of the frontier molecular orbitals of BFI-P2 from the DFT calculations (B3LYP/6-31G(d), 2-decyltetradecyl groups were replaced with methyl groups).

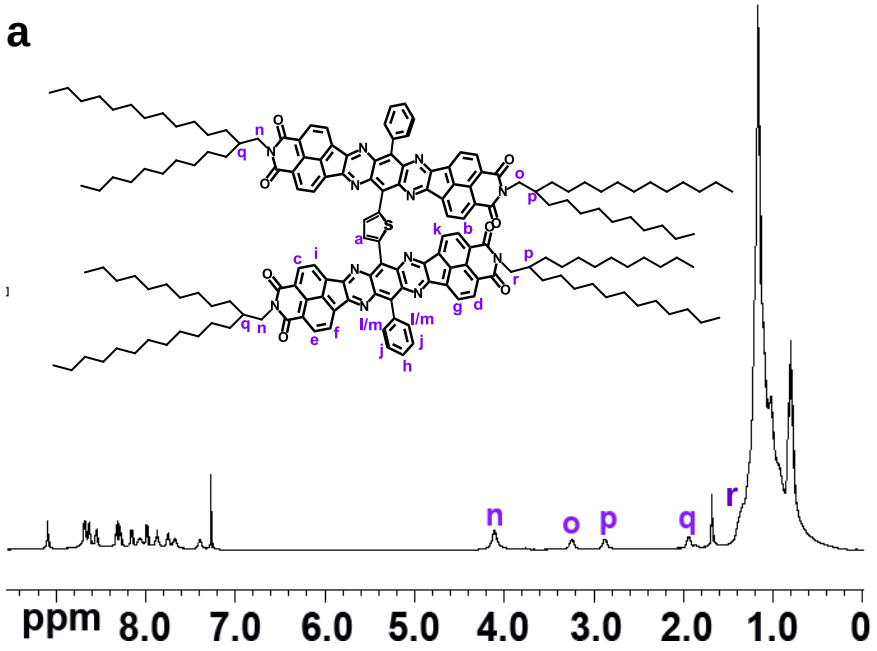

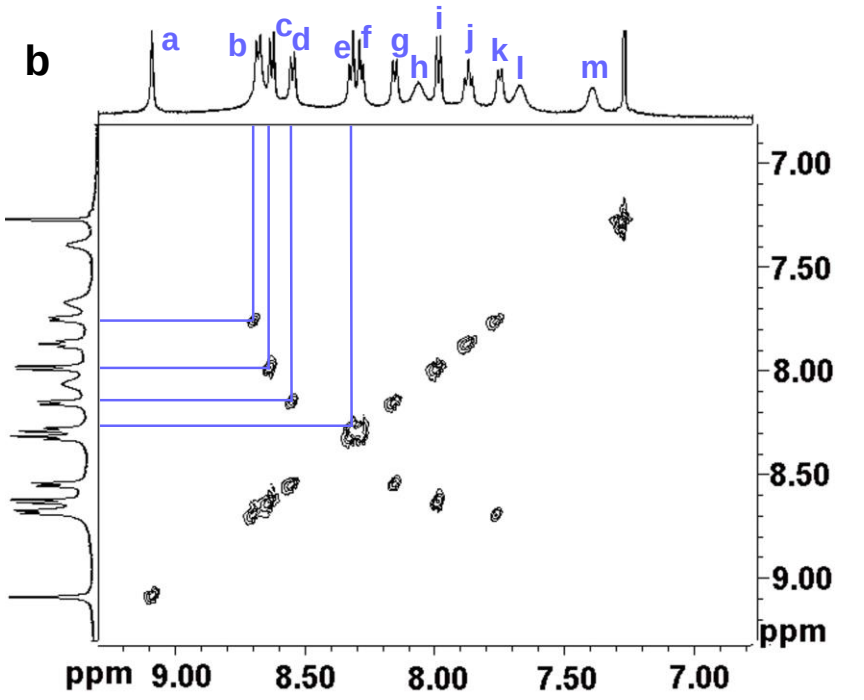
b
a
b
c
d
e
f
g
h
i
j
k
l
m
7.00
7.50
8.00
8.50
9.00
ppm
ppm 9.00
8.50
8.00
7.50
7.00

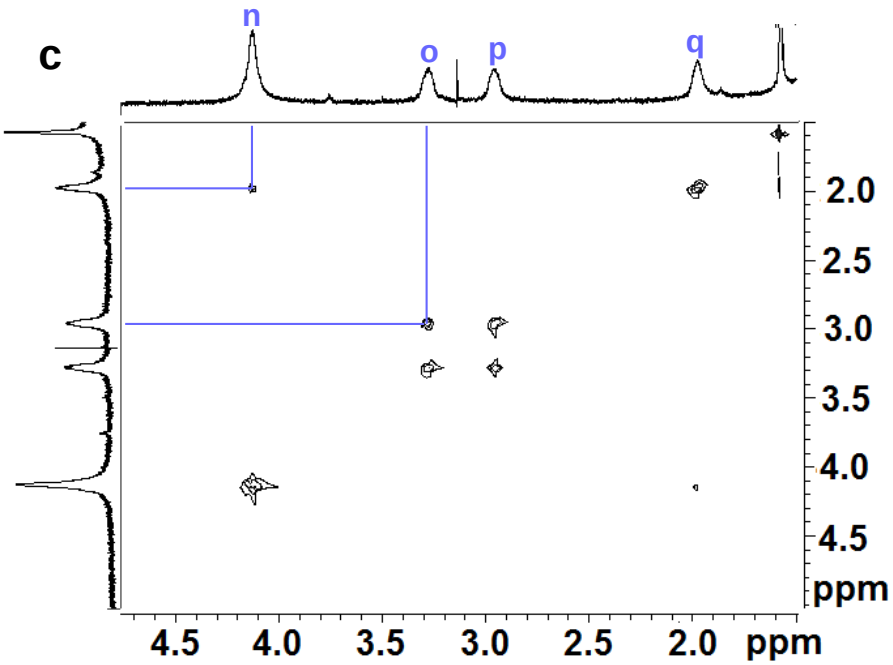
c
n
o
p
q
2.0
2.5
3.0
3.5
4.0
4.5
ppm
4.5
4.0
3.5
3.0
2.5
2.0
ppm

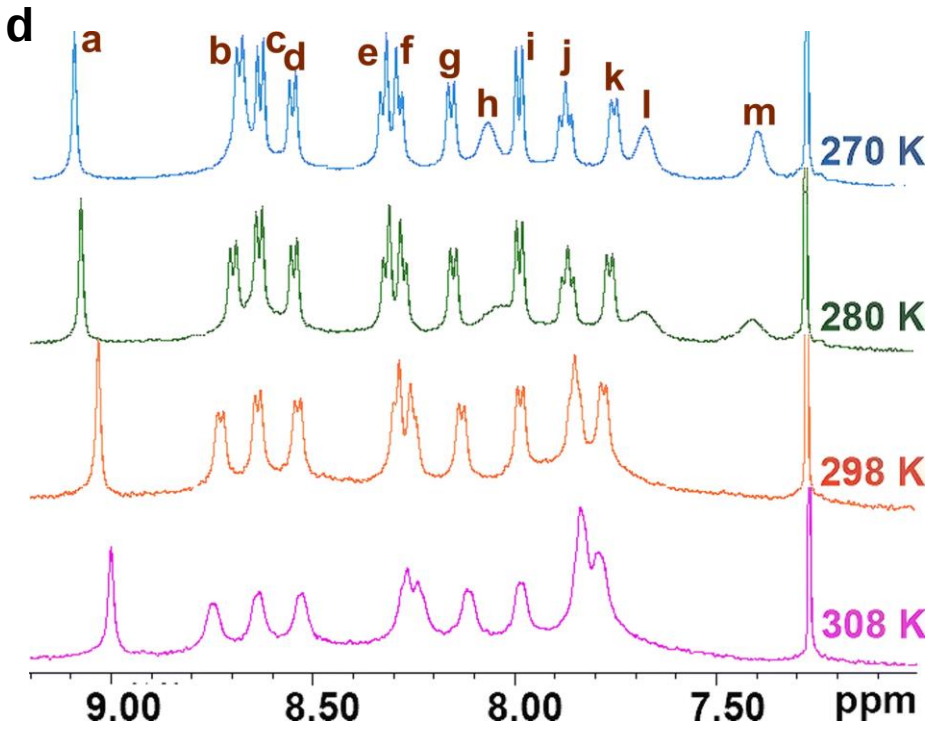

Figure S6. The 1D ^{1}H NMR spectrum and molecular structure of DBFI-T with proton assignments (a), 2D COSY ^{1}H NMR spectrum in the aromatic (b) in the aliphatic (c) regions and variable temperature 1D ^{1}H NMR spectra of DBFI-T in $CDCl_3$ in the temperature range from 270 K to308 K (d).

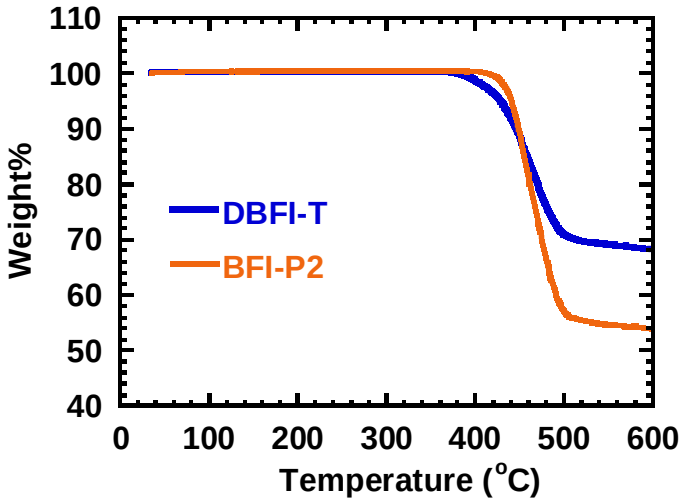

Figure S7. TGA traces of DBFI-T and BFI-P2 (heating at 10 ºC/min under argon).

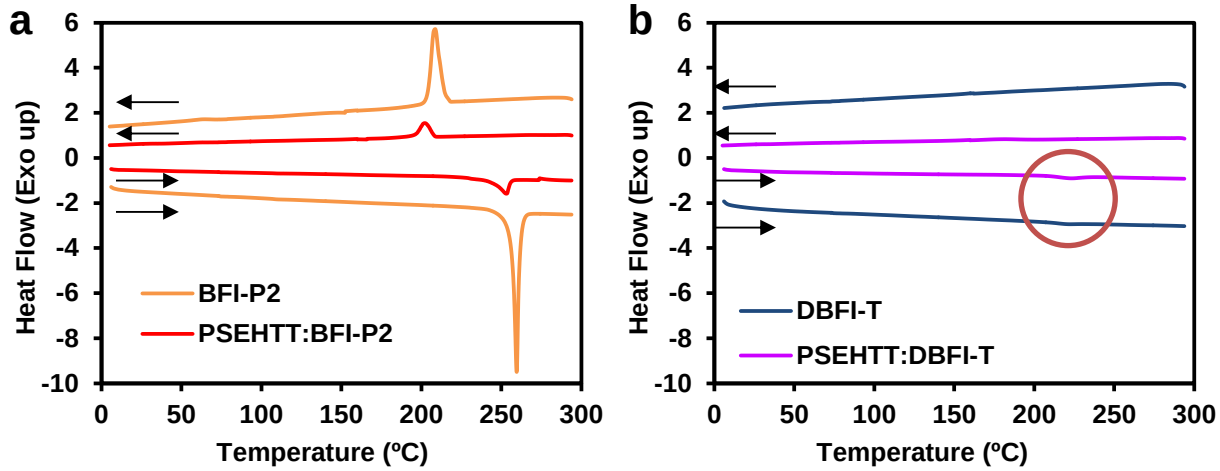

Figure S8. DSC scans of BFI-P2, DBFI-T and PSEHTT:acceptor blends (at 20 ºC/min, under N_2). During heating scans from 0 to 300 ºC, BFI-P2 showed an intense sharp melting peak at T_m = 259 ºC. The corresponding crystallization peak appeared at T_c = 208 ºC during the cooling scans. The same peaks also appeared in the similar range (T_m = 254 ºC and T_c = 203 ºC.) for the PSEHTT:BFI-P2 (1:4 wt/wt) blend under the same conditions, which indicated that BFI-P2 is crystalline in both the neat materials and the PSEHTT:BFI-P2 blend. In contrast, neat DBFI-T and PSEHTT:DBFI-T (1:2 wt/wt) blend only showed a weak, broad transition at T = 224 ºC during the heating suggesting a poor crystalline property of the DBFI-T molecules.

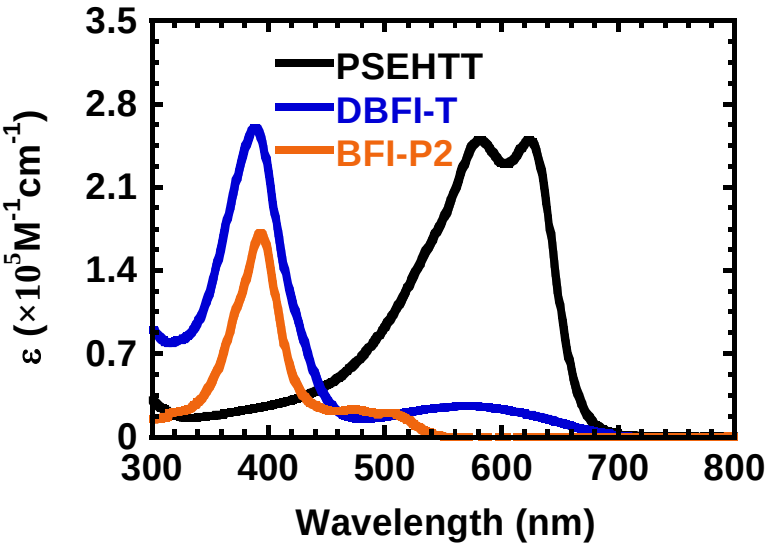

Figure S9. Absorption spectra of DBFI-T, BFI-P2 and PSEHTT in chloroform.

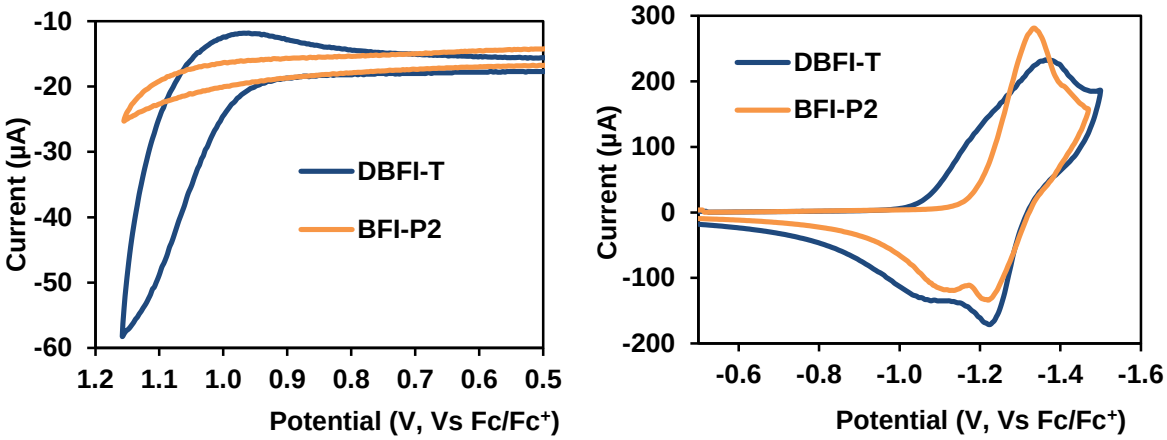

Figure S10. Cyclic voltammograms of DBFI-T and BFI-P2 thin films with ferrocene as the internal reference.

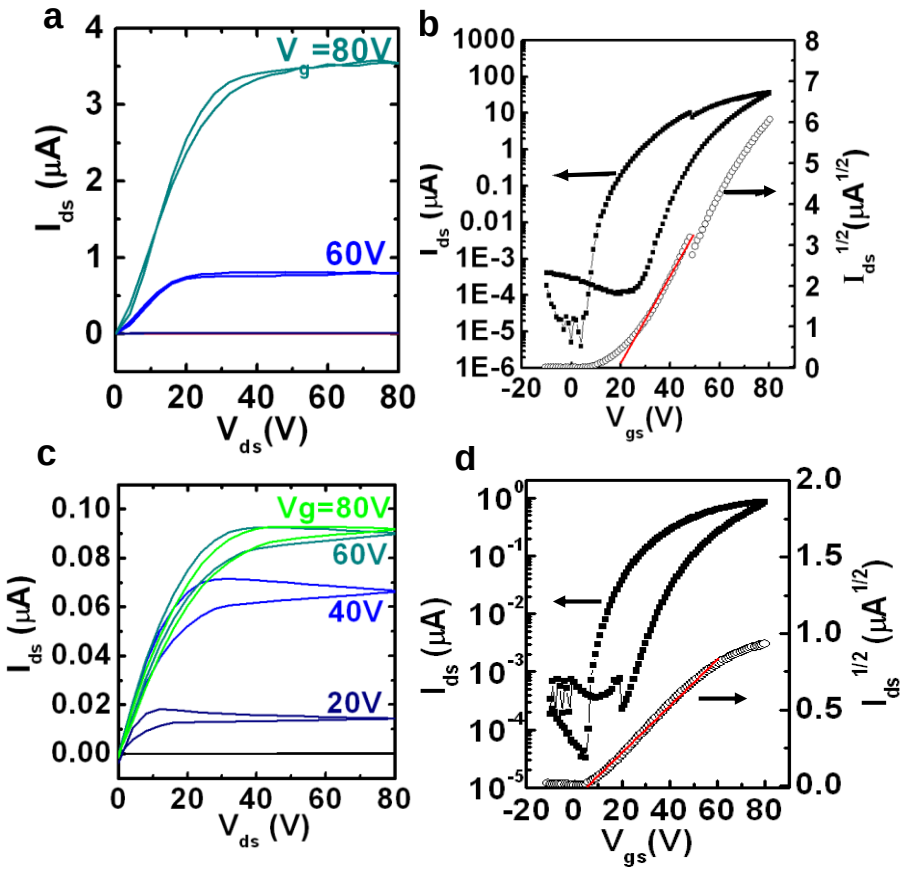

Figure S11. Output and transfer characteristics of BFT-P2 (a and b) and DBFI-T (c and d) OFETs.

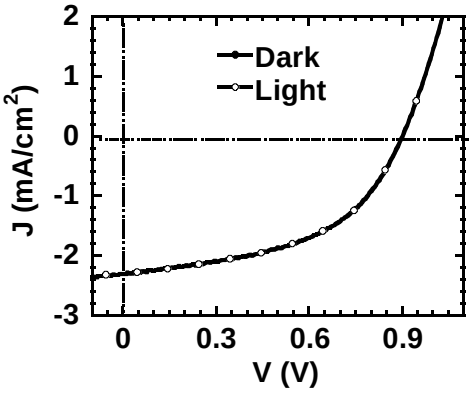

Figure S12. The J-V curve of PSEHTT:BFI-P2 blend (1:4 wt/wt) conventional solar cells.

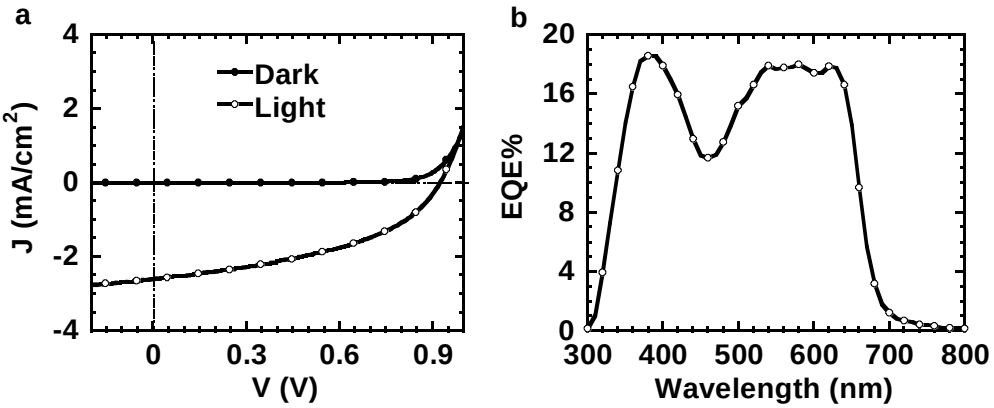

Figure S13. J-V curves (a) and the EQE spectrum (b) of PSEHTT:BFI-P2 blend (1:4 wt/wt) inverted solar cells.

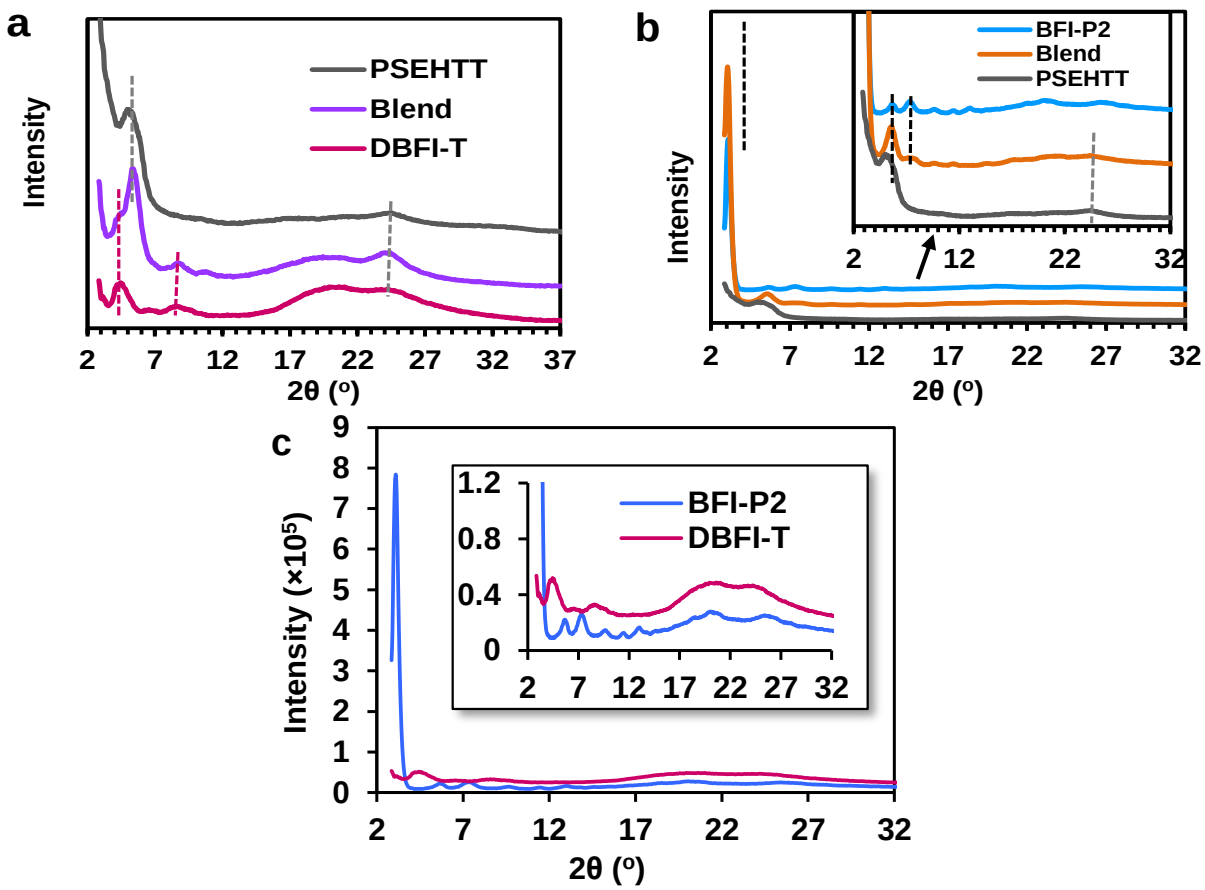

Figure S14. XRD patterns of the drop-cast films of PSEHTT, DBFI-T and the PSEHTT:DBFI-T (1:2 wt/wt) blend (a), PSEHTT, BFI-P2 and the PSEHTT:BFI-P2 (1:4 wt/wt) blend (b), and BFI-P2 and DBFI-T neat films (c).

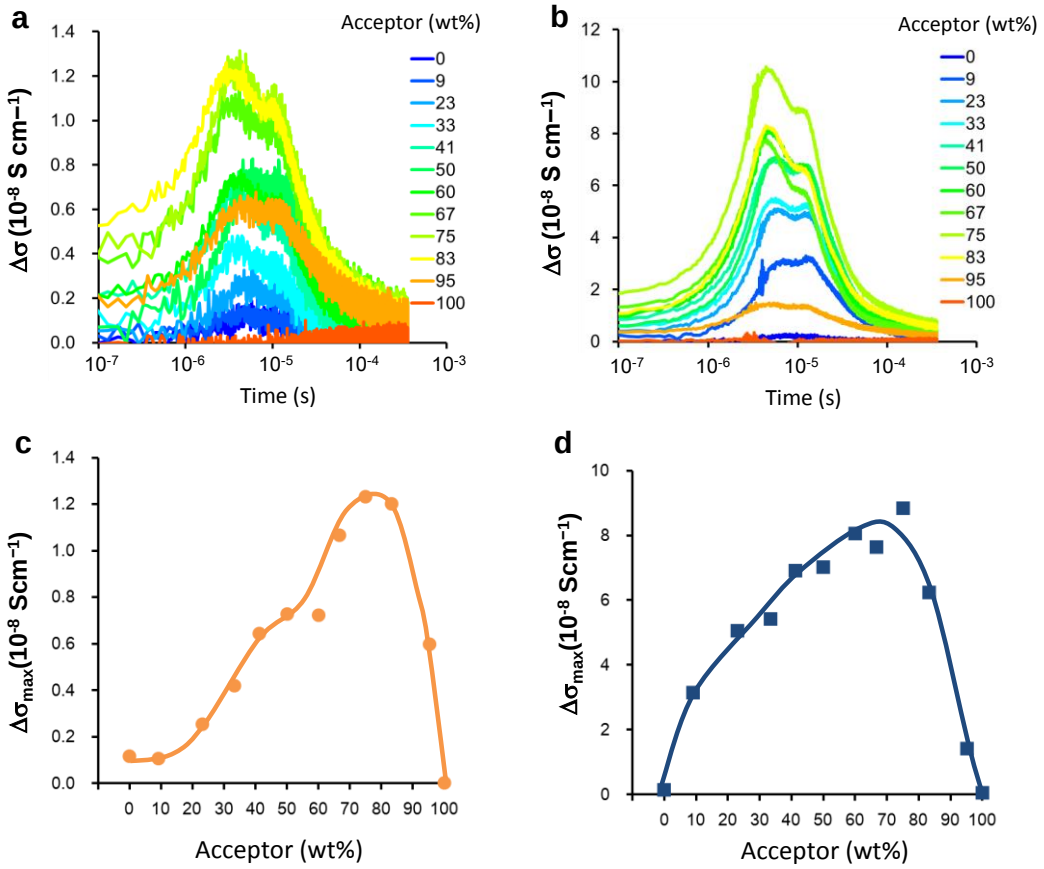

Figure S15. Photoconductivity transients of PSEHTT:BFI-P2 (a) and PSEHTT:DBFI-T (b) blend films measured by Xe-flash TRMC. The acceptor ratio was increased from blue (PSEHTT=100 wt%) to red (PSEHTT=0 wt%). The photoconductivity transient maxima ($\Delta\sigma_{max}$) are plotted as a function of acceptor ratio for PSEHTT:BFI-P2 (c) and PSEHTT:DBFI-T (d). The lines are a guide for the eye.

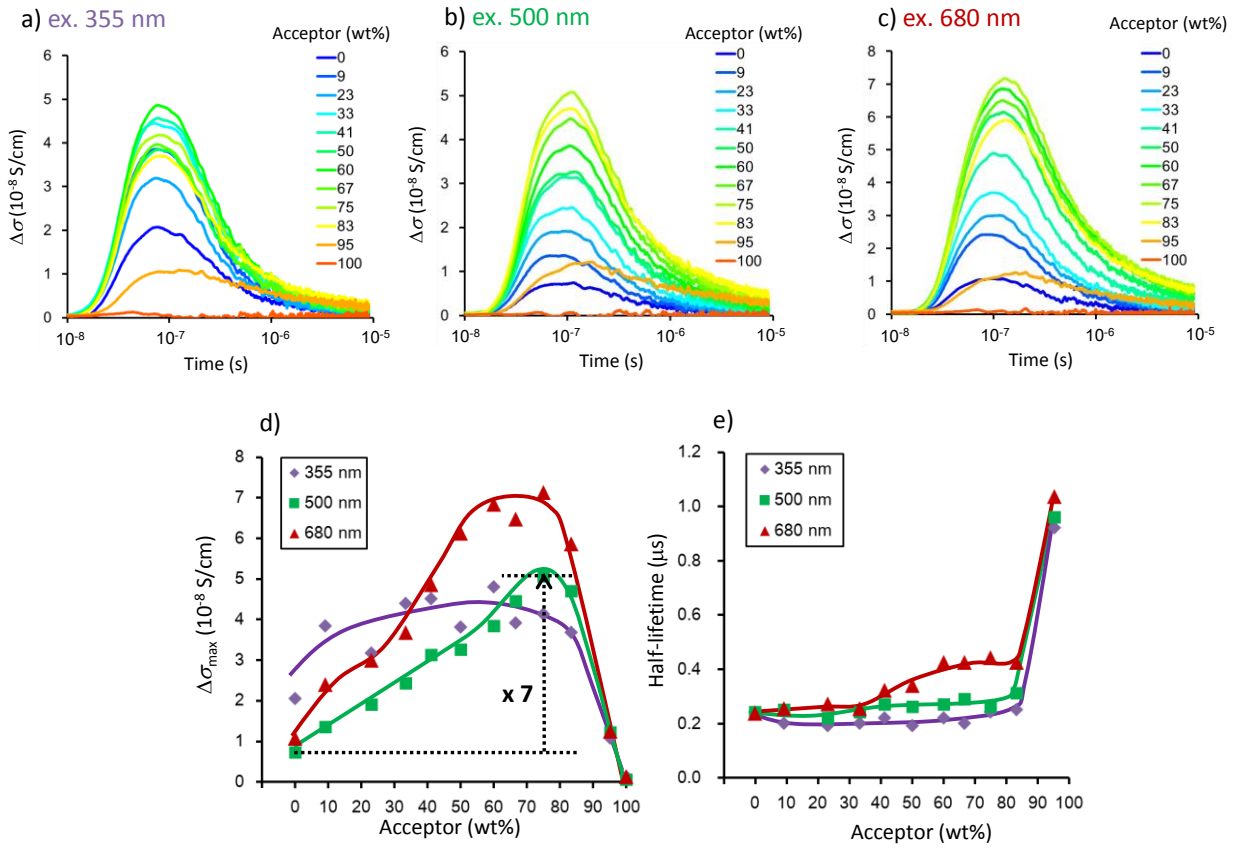

Figure S16. Photoconductivity transients of PSEHTT:BFI-P2 blend films measured by laser-flash TRMC upon excitations at 355 nm (a), 500 nm (b), and 680 nm (c). The acceptor ratio was increased from blue (PSEHTT=100 wt%) to red (PSEHTT=0 wt%). The maxima ($\Delta\sigma_{max}$) (d) and half-lifetime (e) of the photoconductivity transients as a function of acceptor ratio for each excitation wavelength. The lines are a guide for the eye.

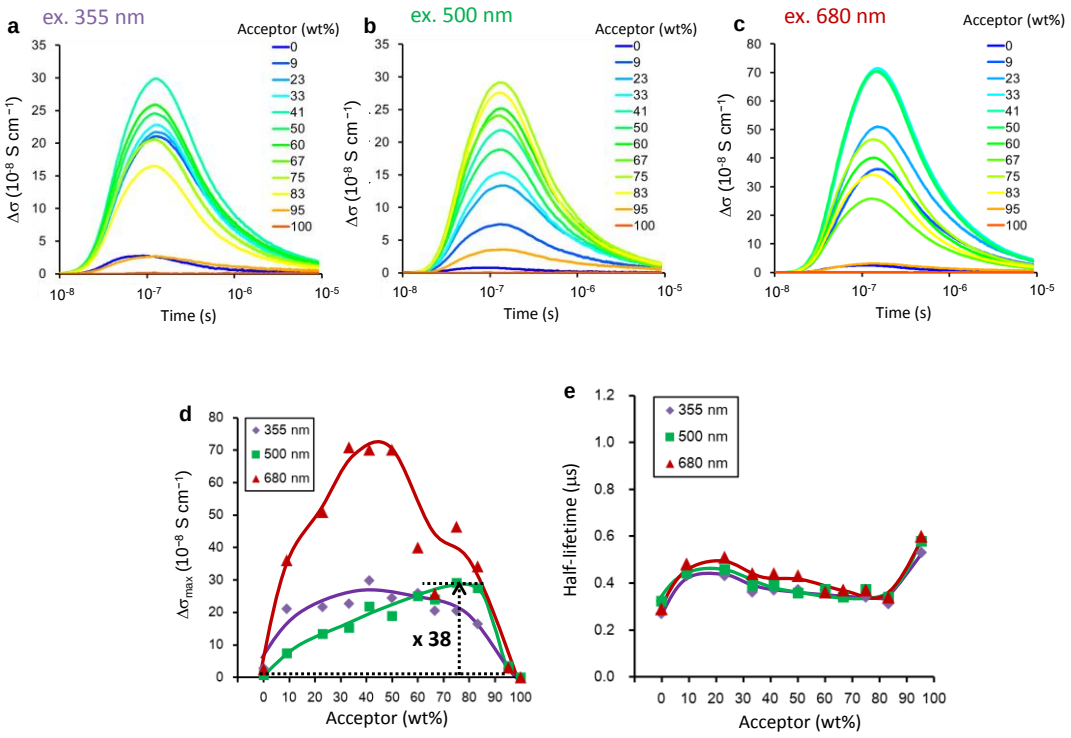

Figure S17. Photoconductivity transients of PSEHTT:DBFI-T blend films measured by laser-flash TRMC upon excitations at 355 nm (a), 500 nm (b), and 680 nm (c). The acceptor ratio was increased from blue (PSEHTT=100 wt%) to red (PSEHTT=0 wt%). The maxima ($\Delta\sigma_{max}$) (d) and half-lifetime (e) of the photoconductivity transients as a function of acceptor ratio for each excitation wavelength. The lines are a guide for the eye.

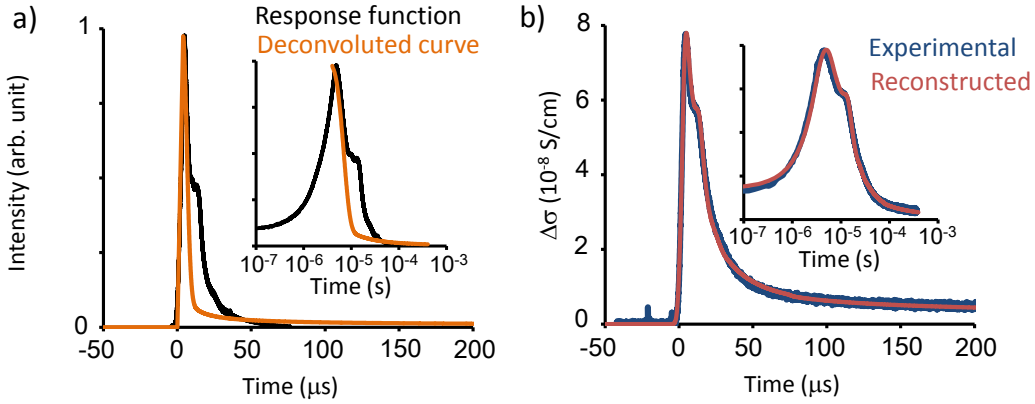

Figure S18. Convolution and deconvolution analyzes of Xe-flash TRMC transients of PSEHTT:DBFI-T =1:2 film. a) The black line is the temporal profile of the white light pulse measured by a Si pin photodetector, which can be regarded as a response function. The orange line is a real function deconvoluted from the response function and the observed decay. The inset

is a semi-logarithmic plot. b) Comparison of experimental decay (blue line) and the decay reconstructed from the real and response functions. The inset is a semi-logarithmic plot.

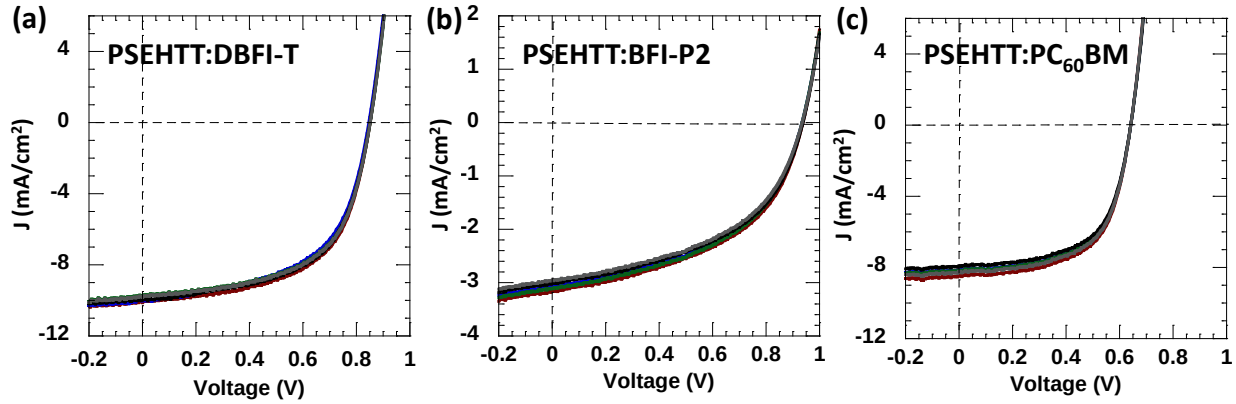

Figure S19. Overlaid J-V curves of 5 inverted devices of each type (a) PSEHTT:DBFI-T, (b) PSEHTT:BFI-P2 and (c) PSEHTT:$PC_{60}BM$ inverted solar cells.

3. Supporting Tables

Table S1. Properties of DBFI-T and BFI-P2.

	λ_{max}[a] (logε) (nm)	λ_{max}[b] (α) (nm) (cm^{-1})	E_g[c] (eV)	LUMO[d] (eV)	HOMO (eV)	T_d[g] (°C)
BFI-P2	505 (4.25) 473 (4.32) 393 (5.23)	515 (1.6×10^4) 495 (1.6×10^4) 374 (8.7×10^4)	2.19	−3.6	<−5.8[f] −5.8[e]	441
DBFI-T	569 (4.43) 389 (5.41)	585 (6.1×10^3) 387 (6.5×10^4)	1.73	−3.8	5.8[f] −5.5[e]	430

[a] In dilute $CHCl_3$ solution. [b] From thin films on glass substrates. [c] Optical band gap, calculated from the absorption edge. [d] Calculated from the onset of the reduction cyclic voltammograms. [e] Calculated from LUMO and E_g, HOMO = LUMO–E_g. [f] Calculated from the onset of the oxidation cyclic voltammograms. [g] Thermal decomposition temperature determined by thermogravimetric analysis (TGA, corresponding to 5% weight loss).

Table S2. Representative geometry parameters of the optimized BFI-P2.

Geometry	BFI-P2
Ph1//BFI (interplanar angle)	59.3°
Ph2//BFI (interplanar angle)	49.8°
N1-N2 (distance)	19.7 Å
C1-C2 (distance)	11.5 Å

The geometries are optimized by DFT calculations at the B3LYP/6-31G(d) level.

Table S3. Representative geometry parameters of the optimized DBFI-T.

Geometry	DBFI-T
Ph1//BFI1 (interplanar angle)	59.3°
BFI1//Th (interplanar angle)	49.8°
Th//BFI2 (interplanar angle)	18.0°
BFI2//Ph2 (interplanar angle)	57.1°
N1-N2 (distance)	19.7 Å
C1-C2 (distance)	19.5 Å

The geometries are optimized by DFT calculations at the B3LYP/6-31G(d) level.

Table S4. Connolly accessible area, Connolly molecular area and Connolly solvent excluded volume of DBFI-T and C_{60}.

	DBFI-T	**C_{60}**
Connolly Accessible Area	1695.974 $Å^2$	528.647 $Å^2$
Connolly Molecular Area	1093.037 $Å^2$	365.092 $Å^2$
Connolly Solvent Excluded Volume	1046.896 $Å^3$	422.739 $Å^3$

The geometries are optimized by DFT calculations at the B3LYP/6-31G(d) level. The Connolly accessible area, Connolly molecular area and Connolly solvent excluded volume of the optimized geometries are calculated using Chem3D Pro (Version 11.0.1).

Table S5. XYZ coordinates of the neutral ground state geometries of DBFI-T (2-decyltetradecyl groups were replaced with methyl groups).

Atom	X	Y	z	Atom	X	Y	z
C	1.991507	4.399565	-0.63513	C	-7.63062	-2.18427	-1.59537
C	1.533988	3.030243	-0.74761	C	-7.57424	-4.59836	-1.39976
C	0.173639	2.691412	-0.52746	C	4.624478	-6.02407	2.232213
C	-0.72127	3.740797	-0.18516	C	5.881507	-1.17335	1.763751
C	-0.25798	5.109722	-0.08304	C	6.014636	-3.54672	2.237268
C	1.097809	5.443607	-0.3052	C	-7.34327	-6.99968	-1.16342
N	-2.03283	3.417007	0.081638	C	-8.29145	-3.40817	-1.6565
C	-2.81866	4.402729	0.406775	C	-8.14186	-5.89202	-1.43297
C	-2.35402	5.785928	0.496351	C	5.975086	-5.93221	2.660241
N	-1.11998	6.127825	0.268323	C	6.617756	-2.26929	2.204356
N	3.307597	4.731575	-0.88164	C	6.667056	-4.72414	2.667183
C	4.097623	3.752961	-1.21388	C	-9.73494	-3.50681	-1.98441

C	3.63395	2.371594	-1.3362	C	-9.58313	-6.01491	-1.75681
N	2.399029	2.024425	-1.11329	C	8.027881	-2.15018	2.645423
C	6.524302	4.746655	-1.61589	C	8.078527	-4.6285	3.114899
C	7.836372	4.354816	-1.99075	N	-10.2758	-4.81229	-2.00791
C	8.15519	3.032988	-2.28986	O	-10.4252	-2.52675	-2.22177
C	7.149591	2.042625	-2.2213	O	-10.1694	-7.08575	-1.81078
C	5.867346	2.440741	-1.84973	N	8.656068	-3.3391	3.069637
C	5.533166	3.781913	-1.5446	O	8.640632	-1.09269	2.653104
C	7.359032	0.67465	-2.50711	O	8.714231	-5.59769	3.501596
C	6.294491	-0.21708	-2.41439	C	-11.7024	-4.95925	-2.32484
C	4.991587	0.202901	-2.03714	C	10.05271	-3.19637	3.501138
C	4.777729	1.541571	-1.74996	C	1.569114	6.85099	-0.19652
C	9.526234	2.624134	-2.68379	C	0.990271	7.862515	-0.97807
C	8.721644	0.242951	-2.90018	C	2.60162	7.194425	0.689442
N	9.706898	1.249632	-2.95952	C	1.436579	9.179037	-0.88148
C	11.049	0.797747	-3.3489	C	3.03774	8.513642	0.795953
O	9.006964	-0.91537	-3.16553	C	2.459406	9.510311	0.008455
O	10.4513	3.417752	-2.7691	C	-0.62103	-6.96649	0.631751
C	-5.00847	8.398639	1.530339	C	0.312298	-7.75897	-0.05425
C	-3.70993	7.970765	1.147939	C	-1.49987	-7.59088	1.530243
C	-3.49645	6.625591	0.897054	C	0.359963	-9.13714	0.146025
C	-4.58238	5.728032	1.033071	C	-1.44265	-8.96723	1.740518
C	-5.86062	6.133331	1.410615	C	-0.51528	-9.74609	1.046553
C	-6.07035	7.507965	1.662777	H	6.311475	5.786823	-1.39234
C	-4.24867	4.379522	0.758806	H	8.627246	5.095007	-2.0521
C	-5.23639	3.41483	0.870878	H	6.483909	-1.26081	-2.64238
C	-6.54421	3.81334	1.253032	H	4.184032	-0.51932	-1.97933
C	-6.86177	5.142228	1.519523	H	11.69992	1.667717	-3.36721
C	-7.42658	7.955284	2.065281	H	11.4139	0.060505	-2.63082
C	-8.22427	5.56588	1.920727	H	11.00889	0.326107	-4.33274
N	-8.40768	6.94279	2.164985	H	-5.19702	9.448068	1.731116
O	-7.6924	9.12481	2.299385	H	-2.90486	8.692567	1.058151
O	-9.15966	4.788909	2.0422	H	-5.02255	2.369132	0.675757
C	-9.76532	7.338331	2.562046	H	-7.33252	3.073668	1.347282
C	-0.31605	1.31292	-0.65238	H	-10.0563	6.800867	3.466619
C	-1.44048	0.888056	-1.33234	H	-10.4726	7.082366	1.770402
S	0.490305	-0.04093	0.099197	H	-9.76069	8.410734	2.737609
C	-1.66913	-0.49572	-1.23112	H	-2.07625	1.55899	-1.89495
C	-0.74392	-1.17866	-0.44619	H	-2.49592	-0.99332	-1.71055
C	-0.74082	-2.60553	-0.11058	H	-5.77051	-1.11634	-1.2425
C	-1.91338	-3.41932	-0.22855	H	3.988494	-0.41737	1.003165
C	0.433706	-3.26599	0.359536	H	-5.37001	-7.75908	-0.64843
C	-1.85727	-4.85391	-0.00761	H	-8.20533	-1.28611	-1.79601

N	-3.11003	-2.82257	-0.54418	H	4.115869	-6.98242	2.241738
C	0.467127	-4.68923	0.61934	H	6.370569	-0.205	1.74933
N	1.548968	-2.5006	0.574356	H	-7.80574	-7.9807	-1.19609
C	-0.67067	-5.49648	0.40953	H	6.499592	-6.82065	2.995947
N	-2.96408	-5.65087	-0.21077	H	-12.1111	-3.96514	-2.48494
C	-4.14612	-3.59827	-0.69232	H	-11.8217	-5.57234	-3.2205
N	1.606351	-5.29901	1.10184	H	-12.2146	-5.45751	-1.49937
C	2.612521	-3.09798	1.030351	H	10.40828	-4.17729	3.80485
C	-4.06482	-5.04652	-0.54785	H	10.11238	-2.49116	4.33253
C	-5.53717	-3.25032	-1.02907	H	10.656	-2.80678	2.678638
C	2.637955	-4.53183	1.300531	H	0.192051	7.611612	-1.6681
C	3.932691	-2.54318	1.36628	H	3.057568	6.42333	1.300776
C	-5.39867	-5.61019	-0.81949	H	0.982993	9.946952	-1.50143
C	-6.24958	-2.08913	-1.282	H	3.831659	8.762245	1.494256
C	-6.21946	-4.49006	-1.09406	H	2.803325	10.5375	0.087695
C	3.978269	-4.87501	1.808062	H	0.996839	-7.2907	-0.75329
C	4.531756	-1.29378	1.340319	H	-2.22432	-6.9914	2.070411
C	4.690185	-3.65166	1.818705	H	1.082908	-9.73515	-0.40123
C	-5.96349	-6.87414	-0.8531	H	-2.12442	-9.43157	2.447178
C	1.991507	4.399565	-0.63513				

Table S6. XYZ coordinates of the neutral ground state geometries of BFI-P2 (2-decyltetradecyl groups were replaced with methyl groups).

Atom	X	Y	z	Atom	X	Y	z
C	-1.21163	0.724519	-0.00647	C	9.196752	-1.25551	-0.05016
C	-1.21168	-0.72434	0.006706	N	9.831583	0.002974	0.00055
C	0	-1.45226	0.000034	O	9.846558	2.301421	0.09142
C	1.211679	-0.72434	-0.00665	O	9.862721	-2.27949	-0.09082
C	1.211627	0.724519	0.006516	C	11.29985	-0.02966	-0.00067
C	0.000001	1.452453	0.000023	C	-1E-06	-2.94081	0.000042
N	2.393901	-1.43505	-0.0408	C	0.654385	-3.65698	1.013774
C	3.487888	-0.73112	-0.02705	C	-0.65439	-3.65699	-1.01368
C	3.487727	0.731487	0.02668	C	0.648249	-5.05054	1.017412
N	2.393737	1.435326	0.040541	C	-0.64826	-5.05055	-1.01731
N	-2.39374	1.435326	-0.0405	C	-7E-06	-5.75246	0.000057
C	-3.48773	0.731488	-0.02664	C	0	2.940997	0.000019
C	-3.48789	-0.73112	0.027102	C	-0.6541	3.657172	1.013935
N	-2.3939	-1.43504	0.040858	C	0.654099	3.657169	-1.0139
C	-5.54432	2.404937	-0.0984	C	-0.64796	5.050731	1.017564
C	-6.96381	2.420263	-0.09836	C	0.647958	5.050729	-1.01753
C	-7.71532	1.249109	-0.05048	C	-1E-06	5.752643	0.000015
C	-7.0549	0.000756	0.000068	H	-4.99106	3.337457	-0.13746
C	-5.66173	0.000581	0.000188	H	-7.49651	3.364677	-0.13704

C	-4.88909	1.185724	-0.04918	H	-7.49762	-3.3636	0.137148
C	-7.71471	-1.24776	0.050472	H	-4.99155	-3.33669	0.137937
C	-6.96444	-2.41935	0.09857	H	-11.6544	0.996828	-0.03762
C	-5.54481	-2.40417	0.098812	H	-11.6582	-0.59259	-0.86362
C	-4.88945	-1.18499	0.049637	H	-11.6581	-0.52706	0.904155
C	-9.19867	1.265961	-0.05076	H	7.496509	3.364672	0.137077
C	-9.19675	-1.25552	0.049824	H	4.991064	3.337455	0.137466
N	-9.83158	0.002981	-0.0005	H	4.991545	-3.33669	-0.13793
C	-11.2998	-0.02965	0.000624	H	7.497617	-3.3636	-0.13729
O	-9.86272	-2.2795	0.090551	H	11.65814	-0.59435	0.862438
O	-9.84656	2.301416	-0.09167	H	11.65442	0.996746	0.039569
C	6.963808	2.42026	0.098371	H	11.65821	-0.52523	-0.9052
C	5.544325	2.404935	0.098402	H	1.162905	-3.11636	1.80466
C	4.889093	1.185722	0.049209	H	-1.16291	-3.11637	-1.80457
C	5.661728	0.000579	-0.00016	H	1.152159	-5.58816	1.815431
C	7.054899	0.000753	-6.2E-05	H	-1.15217	-5.58817	-1.81532
C	7.715318	1.249104	0.050523	H	-9E-06	-6.83862	0.000064
C	4.889447	-1.185	-0.0496	H	-1.16239	3.116548	1.804974
C	5.544811	-2.40417	-0.0988	H	1.162386	3.116543	-1.80494
C	6.964442	-2.41935	-0.09862	H	-1.15164	5.58835	1.815726
C	7.714706	-1.24776	-0.05055	H	1.151635	5.588344	-1.8157
C	9.198672	1.265948	0.050962	H	-1E-06	6.838799	0.000013
C	-1.21163	0.724519	-0.00647	C	9.196752	-1.25551	-0.05016
C	-1.21168	-0.72434	0.006706	N	9.831583	0.002974	0.00055
C	0	-1.45226	0.000034	O	9.846558	2.301421	0.09142
C	1.211679	-0.72434	-0.00665	O	9.862721	-2.27949	-0.09082
C	1.211627	0.724519	0.006516	C	11.29985	-0.02966	-0.00067
C	0.000001	1.452453	0.000023	C	-1E-06	-2.94081	0.000042
N	2.393901	-1.43505	-0.0408	C	0.654385	-3.65698	1.013774
C	3.487888	-0.73112	-0.02705	C	-0.65439	-3.65699	-1.01368
C	3.487727	0.731487	0.02668	C	0.648249	-5.05054	1.017412
N	2.393737	1.435326	0.040541	C	-0.64826	-5.05055	-1.01731
N	-2.39374	1.435326	-0.0405	C	-7E-06	-5.75246	0.000057
C	-3.48773	0.731488	-0.02664	C	0	2.940997	0.000019
C	-3.48789	-0.73112	0.027102	C	-0.6541	3.657172	1.013935
N	-2.3939	-1.43504	0.040858	C	0.654099	3.657169	-1.0139
C	-5.54432	2.404937	-0.0984	C	-0.64796	5.050731	1.017564
C	-6.96381	2.420263	-0.09836	C	0.647958	5.050729	-1.01753
C	-7.71532	1.249109	-0.05048	C	-1E-06	5.752643	0.000015
C	-7.0549	0.000756	0.000068	H	-4.99106	3.337457	-0.13746
C	-5.66173	0.000581	0.000188	H	-7.49651	3.364677	-0.13704
C	-4.88909	1.185724	-0.04918	H	-7.49762	-3.3636	0.137148
C	-7.71471	-1.24776	0.050472	H	-4.99155	-3.33669	0.137937

C	-6.96444	-2.41935	0.09857	H	-11.6544	0.996828	-0.03762
C	-5.54481	-2.40417	0.098812	H	-11.6582	-0.59259	-0.86362
C	-4.88945	-1.18499	0.049637	H	-11.6581	-0.52706	0.904155
C	-9.19867	1.265961	-0.05076				

4. References

1 Frisch, M. J. *et al. Gaussian, Inc., Wallingford CT, 2009.*

2 Murgatroyd, P. N. Dimensional considerations for space-charge conduction in solids. *J. Phys. D: Appl. Phys.* **3**, 1488-1490 (1970).